On the selection of advanced signal processing techniques for guided wave damage identification using a statistical approach

Ching-Tai Ng

School of Civil, Environmental & Mining Engineering, The University of Adelaide, SA, 5005, Australia. (Tel: +61 08 8131 1237) (Email: alex.ng@adelaide.edu.au)

Abstract

Advanced signal processing techniques are widely used to detect damage in structures. The current study proposed a statistical approach to the identification of structural damages using guided waves. Various signal processing techniques were applied in order to determine and improve the ways in which damage in a structure can be identified for remediation. The proposed statistical approach not only provides a quantitative identification of the damages, but can also quantify the uncertainties associated with the damage identification results. This allows the performance of various signal processing techniques to be evaluated and compared in terms of accuracy and the degree of uncertainty associated with the damage identification results. Damage identification was initially conducted using time domain guided wave signals so that the results could be used as a benchmark. Four signal processing techniques were then considered. Hilbert transform was used to extract the signal envelopes. Fast Fourier transform was applied to transform the guided wave signals from the time domain to the frequency domain. Gabor wavelet transform was employed to extract the wavelet coefficients from time-frequency domain. Discrete wavelet transform was used to decompose the guided wave signals. The frequency domain signal, signal envelopes, wavelet coefficients and discrete wavelet decomposed signals were then employed separately to identify the damages in conjunction with the proposed statistical damage identification approach. Laboratory experiments were conducted and the data were used to verify the proposed statistical

approach. The levels of accuracy and degree of uncertainty associated with the damage identification results by each of the signal processing techniques were compared in detail. The results reported in this paper show that a suitable signal processing technique combined with the proposed statistical approach produces more robust identification of damages in a structure.

Keywords:

Damage identification; statistical approach; signal processing; Fourier transform; Hilbert transform; wavelet transform; guided waves; probability density function

1. Introduction

1.1. Overview

Identifying damage at its early stage is paramount to maintaining the safety and integrity of structures and reducing the risk of catastrophic failure. The development of robust and cost effective damage identification techniques to guarantee the safety of structures has therefore always been of particular interest in engineering. In the last two decades, with the refinement of computers and sensors, a variety of sophisticated damage identification techniques has been developed to ensure structural integrity and safety [1-4].

Vibration-based damage identification methods [5-11], which rely on low-frequency vibration characteristics of structures to identify damages, have been extensively investigated, for example, especially in the fields of civil and mechanical engineering. Although low-frequency vibration methods can be used to globally monitor structures, they are generally not sensitive to local incipient damages [4], however, which means that damages as small as a centimeter and can threaten the safe operation of structures. For example, metal corrosions and fatigue cracks are hard to be detected and are potential lead to catastrophic failure in the structural components of engineering structures, such as bridges, planes, oil platforms and trains. These incipient damages are not easy to identify. Therefore, in recent years, high-frequency approaches have been explored, such as guided wave propagation [12], acoustic emission [13] and impendence measurements [14].

Guided waves have been widely recognized to be promising for damage detection. They are elastic waves whose propagation characteristics depend on structural boundaries. The excitation frequencies of these waves are at several hundred kilohertz and the corresponding wavelengths are of the order of millimeters. Since, in general damage can be identified if the wavelengths are of the same order as the damage size, guided waves are sensitive to small damages. Furthermore, guided waves can propagate over long distances with little loss of energy, making them ideal for large area and cross sectional monitoring of structures and cost effective [12]. In recent years a significant amount of research has been carried out to

investigate their use [15-20].

1.2. Damage identification using guided waves

Damage identification can be described as a four-level process [4] that aims to determine (i) the existence of damage, (ii) the location of damage, (iii) the type of damage and (iv) the severity of the damage.

In general the existence and location of damage can be identified from guided wave data without additional information. For example, damage can be expected when guided wave reflected from the damage is observed in the measured signals, and the location of the damage can be identified by using the arrival time of the reflected wave [12]. However, additional information is essential for determining the type of damage and its severity. In practice, the types of damages common to structures of various material compositions can be pre-determined by an experienced engineer, and only a limited number of sensors is installed on the structural component.

In terms of actually determining damage location [21-23] and extent [24-26], a number of techniques have been developed, particularly in two-dimensional waveguides, such as plates and shells. Relatively less research work has focused on quantitative identification of damages in one-dimensional waveguides, such as rods and beams.

For determining the severity of damages in one-dimensional waveguides with a limited number of sensors, pattern recognition and optimization are two commonly used approaches. Pattern recognition approach, such as supervised learning [27,28], applies prior experience to make sense of new data in the damage identification. Optimization approach [29-32] minimizes the discrepancy between the numerically predicted structural responses and the measured data by altering the damage parameters of a pre-defined model in order to determine the location and severity of the damage in the structure being tested.

1.3. Signal processing techniques for guided wave-based damage identification

Pattern recognition, optimization and most other damage identification methods use the relationship between the structural condition and the damage information contained in the measured data to identify the damage. The process therefore fully relies on information of damage contained in the data provided by the sensors. In practice, the number of sensors that can be installed on the structure is limited and the measured data is usually contaminated by noise. Data pre-processing is necessary to extract the information of damage from the data in order to maximize the performance of damage identification. Staszewski [33] discussed the importance of applying signal processing techniques in damage identification when using a pattern recognition approach. Since pattern recognition has difficulty in dealing with data of high dimensionality, signal processing techniques are generally used for feature extraction and data compression.

Different from pattern recognition, signal processing techniques for the optimization approach do not aim to compress the data, but to improve the sensitivity of the measured guided wave signals to the damage. Yu and Giurgiutiu [34] have demonstrated that the application of advanced signal processing techniques, such as Hilbert transform, continuous wavelet transform and discrete wavelet transform, improves the performance of using the guided waves to locate the damages following a phased-array approach. In general these signal processing techniques have not been specifically developed for data compression, they are suitable for improving the performance of the optimization approach in damage identification.

The study reported in this paper therefore had two main objectives. The first was to enhance the guided wave-based quantitative identification of damage following optimization by applying signal processing techniques. The other objective was to evaluate the performance of the advanced signal processing techniques, such as Hilbert transform, Fast Fourier transform, Gabor wavelet transform and discrete wavelet decomposition, in terms of damage identification. This was achieved by comparing the level of accuracy and degree of uncertainty associated with the damage identification results by each of the signal processing

techniques. All data used in the present study were from actual guided wave signals measured in experiments conducted in laboratory.

The paper is organized as follows. A statistical framework for damage characterization is first presented in Section 2. The framework was developed using a Bayesian approach, which not only provides quantitative identification of the damage but also allows the uncertainty associated with the damage identification results to be quantified. The experimental setup used to collect the guided wave signals in damaged beams is then described in detail in Section 3. In Section 4 a computationally efficient spectral finite element method is described. The proposed method is used to model damaged beams for damage identification using the proposed statistical approach. Various advanced signal processing techniques for enhancing damage identification are presented in the Section 5. The results of the damage identification and the performance of each advanced signal processing technique are then compared and discussed in detail. Conclusions are presented in Section 6.

2. Statistical framework for damage identification

The current study employed a statistical damage identification framework in conjunction with the damaged beams modeled by the spectral finite element method. The model was able to describe the relationship between the condition of the structure and the information about the damage provided by the guided waves. The damage is identified by changing the damage parameters to minimize the discrepancy between the predicted and the measured guided wave signals. In reality no numerical model can be expected to offer perfect predictions, the number of sensors that can be installed on the structures is always limited and the measured data usually contaminated by noise. Hence any damage identification will produce uncertainties. In addition to quantifying the damages, it is also important to explicitly quantify the uncertainties associated with the damage identification results, which provides valuable information for engineers attempting to undertake appropriate remedial work. In this

study the performance of the signal processing techniques was assessed not only in terms of how accurate the results were, but also in terms of the uncertainties in the damage identification.

2.1. Bayesian statistical framework

The proposed statistical framework was based on the Bayesian statistical framework [35]. Different from most of the existing optimization approaches, the Bayesian statistical framework identifies damages by maximizing the posterior probabilistic density function (PDF) of a damage scenario, conditional on the measured data. The Bayesian statistical framework consists of a set of probability models $p(D|\boldsymbol{\alpha},M)$ that describes the data of a structure with uncertain parameters $\boldsymbol{\alpha}=[\boldsymbol{\theta},\sigma]^T\in\Theta\subset{}^{\circ}{}^{N_p+1}$ and a prior probability model $p(\boldsymbol{\alpha}|M)$ that represents the initial probability of each model. This arrangement allows for predictions of guided wave signals and modeling of prediction error $e(t,\boldsymbol{\theta})$. The prediction error $e(t,\boldsymbol{\theta})$ is defined as the difference between the prediction and the measurement, which may be the result of measurement noise and modeling error. N_p is the dimension of $\boldsymbol{\theta}$ which represents the parameters used to describe the damage scenario. Prior probability incorporates existing knowledge of the structure, such as the locations more likely to be damaged. D is the available data relating to excitation and the measured guided wave signals. M is the class of the model defined by the value of the uncertain parameters $\boldsymbol{\alpha}$. The fundamental idea of the Bayesian statistical framework is to use data D to update the probability distribution over the uncertain parameters $\boldsymbol{\alpha}$ to give the posterior PDF $p(\boldsymbol{\alpha}|D,M)$ based on the Bayes' theorem [35]

$$p\left(\boldsymbol{\alpha}|D,M\right)=c^{-1}p\left(D|\boldsymbol{\alpha},M\right)p\left(\boldsymbol{\alpha}|M\right) \tag{1}$$

where $c=p(D|M)=\int_{\Theta}p(D|\boldsymbol{\alpha},M)p(\boldsymbol{\alpha}|M)d\boldsymbol{\alpha}$. $p(\boldsymbol{\alpha}|M)$ is the prior PDF specified by M to quantify the initial plausibility of each model defined by the value of $\boldsymbol{\alpha}$. The prior PDF is assumed to be $\pi\left(\boldsymbol{\theta},\sigma\right)$ which is a slowly varying PDF that roughly reflects the engineer's judgments regarding the relative plausibility of different values of $\boldsymbol{\alpha}$ and is

mathematically convenient.\ It is common that the signal-to-noise ratio of the measured guided wave signals is improved by averaging the signals over number acquisitions. Hence the measurement nosie is generally small and the prediction error $e(t,\boldsymbol{\theta})$ is mainly due to the modeling error. It is assume that the prediction error $e(t,\boldsymbol{\theta})$, which is the discrepancy between predicted signals simulated by the numerical model and experimentally measured signals, is norally distributed and can be approximated by Gaussian distribution. In this cse the likelihood $p(D\,|\,\boldsymbol{\alpha},M)$ that represents the probability of getting data based on a given model with $\boldsymbol{\alpha}$ and model class M is defined as

$$p(D\,|\,\boldsymbol{\alpha},M)=\frac{1}{\left(\sqrt{2\pi}\sigma\right)^{N_tN_o}}\exp\left[-\frac{N_oN_t}{2\sigma^2}J\left(\boldsymbol{\theta};D,M\right)\right] \tag{2}$$

where N_o and N_t are the total number of measurement points and time steps. σ is the variance. The function $J(\boldsymbol{\theta};D,M)$ is the contribution of the measured data, and is given by

$$J\left(\boldsymbol{\theta};D,M\right)=\frac{1}{N_oN_t}\sum_{j=1}^{N_o}\sum_{t=1}^{N_t}\left[\hat{q}^{(j)}\left(t\right)-q^{(j)}\left(t;\boldsymbol{\theta},M\right)\right]^2 \tag{3}$$

where $\hat{q}^{(j)}(t)$ is the measurement at j-th location and time t. $q^{(j)}(t;\boldsymbol{\theta},M)$ is the prediction given by the value of $\boldsymbol{\theta}$. When a uniform prior PDF (non-informative prior) is chosen, the most probable parameter $\hat{\boldsymbol{\theta}}$ is obtained by maximizing the posterior PDF in Eqs. (2), which is equivalent to minimizing $J(\boldsymbol{\theta};D,M)$ in Eqs. (3).

The main objective of the Bayesian statistical framework is to obtain the posterior PDF of $\boldsymbol{\theta}$, which is used to describe the damage scenario for a given set of measured data D and a given model class M. This can be calculated from Eq. (1) by integrating the posterior PDF with respect to the σ and it can be approximated as [36]

$$p\left(\boldsymbol{\theta}\,|\,D,M\right)=c_1J\left(\boldsymbol{\theta};D,M\right)^{\frac{N_oN_t-1}{2}}\pi\left(\boldsymbol{\theta},\hat{\boldsymbol{\theta}}(\boldsymbol{\theta})\right) \tag{4}$$

where $\hat{\sigma}^2(\boldsymbol{\theta})=J(\boldsymbol{\theta};D,M)$ and c_1 is a normalizing constant. For identifiable situation [35], $p\left(\boldsymbol{\theta}\,|\,D,M\right)$ becomes negligible everywhere, except for a finite number of locations in the parameter space where the corresponding values of $J(\boldsymbol{\theta};D,M)$ are globally minimized.

2.1.1. Optimization algorithm

As $J(\boldsymbol{\theta};D,M)$ is known only implicitly and is highly nonlinear, a robust numerical optimization algorithm plays an important role in determining the most probable parameter $\boldsymbol{\theta}$. In this study a hybrid optimization algorithm composed of the particle swarm optimization algorithm (PSO) and simplex search method was proposed to determine the global optimal solution. The hybrid optimization algorithm minimizes $J(\boldsymbol{\theta};D,M)$, which is equivalent of maximizing $p(\boldsymbol{\theta}|D,M)$, by changing the value of the parameters $\boldsymbol{\theta}$ that represent the damage scenario. In the proposed hybrid optimization algorithm, the PSO algorithm is first used to determine the local potential space in Θ and then the simplex search method is used to accurately determine the global optimal solution. As the simplex search method is more computationally efficient than the PSO algorithm in its manner of local exploitation, it adds improved efficiency to the proposed method for determining the global optimal solution.

The PSO algorithm is a population-based optimization technique based on the idea of a particle swarm. The algorithm's behavior simulates coordinated social behavior among living organisms [37]. In PSO a set of particles is randomly initialized in the search space under consideration Θ. Each individual of a particle swarm consists of three N_p dimensional vectors, which are the current location $\boldsymbol{\theta}_i$, previous best location $\overline{\boldsymbol{\theta}}_i$ and velocity $\mathbf{v}_i$ of the particle. The current location of each particle is used to evaluate $J(\boldsymbol{\theta};D,M)$ and the best position identified up to that point is stored in the vector $\overline{\boldsymbol{\theta}}_g$ for comparison with the results of later iterations. The velocity and location of each particle are then updated based on its own current and the best location so far with some random perturbations. Each run of the new algorithm can be considered complete after the velocities and locations of all particles have been updated. The equations used to update the velocities and locations of the particles are shown in Fig. 1.

[Fig. 1. Flowchart of PSO algorithm]

In the PSO algorithm the inertia weight w_i at i-th iteration was employed to update the

particle velocities as shown in Fig. 1. In the present study, the inertia weight at the (i+1)-th iteration was chosen as the dynamic variation, with a linear decrease in each iteration [38] as

$$w_{i+1} = w_I - \frac{w_I - w_F}{N_I} i \tag{5}$$

where w_I= 0.9 and w_F=0.4 are the initial weight and final weight satisfying the stability condition $0.5(\lambda_1 + \lambda_2) - 1 < w_{i+1} < 1$. In Fig. 1 R_1 and R_2 are random numbers calculated from a uniform distribution on interval [0,1]. λ_1 and λ_2 are the cognitive and social coefficients for reflecting the degree of confidence in the best solution found by each individual particle and by the swarm as a whole. $\lambda_1 = 0.5$ and $\lambda_2 = 1.25$ were chosen in this study to satisfy the stability condition $0 < (\lambda_1 + \lambda_2) < 4$ [38].

Iteration continues until the maximum number of iterations N_I or sufficient goodness of fit is observed. Fig. 1 shows a summary of the PSO algorithm. The simplex search method is then applied to accurately determine the global optimal solution by using the local potential space identified from the PSO algorithm as the initial trials.

2.1.2. Approximation of the posterior probability density function

Once all the finite number of optimal points $\hat{\boldsymbol{\theta}}_k$, $k = 1,...,K$, is determined using the hybrid optimization algorithm, the posterior PDF $p(\boldsymbol{\theta} \mid D, M)$ can be approximated as a weighted sum of a Gaussian distribution centered at K optimal points [37] as

$$p(\boldsymbol{\theta} \mid D, M) \approx \sum_{k=1}^{K} w_k \mathbf{N}\left(\hat{\boldsymbol{\theta}}_k, \mathbf{A}^{-1}\left(\hat{\boldsymbol{\theta}}_k\right)\right) \tag{6}$$

where $\hat{\boldsymbol{\theta}}_k$ and $\mathbf{A}^{-1}(\hat{\boldsymbol{\theta}}_k)$ are the mean (optimal point) and covariance matrix of a multivariate Gaussian distribution $\mathbf{N}$. The covariance matrix $\mathbf{A}^{-1}(\hat{\boldsymbol{\theta}}_k)$ is the Hessian matrix of the function $N_J \ln J(\boldsymbol{\theta}; D, M)$, where $N_J = (N_o N_t - 1)/2$, evaluated at $\hat{\boldsymbol{\theta}}_k$. The weighting coefficients in Eq. (6) can be calculated as

$$w_k = \frac{\pi\left(\hat{\boldsymbol{\theta}}_k\right)\left|\mathbf{A}^{-1}(\hat{\boldsymbol{\theta}}_k)\right|^{\frac{1}{2}}}{\sum_{k=1}^{K} \pi\left(\hat{\boldsymbol{\theta}}_k\right)\left|\mathbf{A}^{-1}(\hat{\boldsymbol{\theta}}_k)\right|^{\frac{1}{2}}} \tag{7}$$

While calculating the posterior PDF $p(\boldsymbol{\theta} \mid D, M)$ of the parameter $\boldsymbol{\theta}$, which describes the

damage, and the associated uncertainties can be quantified to provide valuable information for engineers who are making decision about remediation. Sections 3 and 4 describe the experimental setup for collecting the actual guided wave signals and a computationally efficient spectral finite element model, respectively. The experimentally collected data were processed by the signal processing techniques described in Section 5. The data and the spectral finite element model were then used in the proposed statistical framework to quantify the damage. In this study the accuracy of the results and the uncertainty were used as reference points by which to assess the performance of the Hilbert transform, Fast Fourier transform, Gabor wavelet transform and discrete wavelet decomposition in the damage identification.

3. Experiments

In this study the experimentally measured guided wave signals were used to demonstrate the capability of the proposed statistical approach in the damage identification and assess the performance of each of the signal processing techniques described in Section 5. The guided wave signals were collected using the experimental setup shown in Fig. 2. Three aluminum beams with a cross-section of 12×6 mm^2 and a length of 2 m were used in the experiments. Each aluminum beam contained a step damage that was used to simulate corrosion. As shown in Fig. 2, each of the beams had a rectangular piezoceramic transducer (Ferroperm Pz27) bonded to the beam end to generate the longitudinal guided wave. A 4 mm thick rectangular backing mass was attached to the piezoceramic transducer to improve the excitability of the longitudinal wave.

The excitation signal was a narrow-band eight-cycle sinusoidal tone burst pulse modulated by a Hanning window. The excitation frequency was 80 kHz as this frequency signal displayed the best signal-to-noise ratio. The excitation signal was generated by a computer controlled function generator (Stanford Research DS345) with 10 V peak-to-peak output voltages. The generated signal was then amplified by a power amplifier (Krohn Hite

model 7500) by a factor of 10-50 before sending it to the piezoceramic transducers. The longitudinal guided wave was then measured using a Laser Doppler vibrometer (OFV 303/OFV 3001, Polytech GmbH). The laser head of the Laser Doppler vibrometer was positioned by a computer controlled positioning system (Newport ESP 300).

As the longitudinal guided wave propagation induced an out-of-plane motion due to the Poisson effect, the longitudinal wave was measured through the out-of-plane displacement using the Laser Doppler vibrometer. As shown in Fig. 2 the measurement point was at the mid-plane of the shorter side of the beam cross-section since the out-of-plane motion of the longitudinal wave was more pronounced at the shorter side and the flexural wave induced due to the effect of mode conversion at the step damage has zero magnitude at the mid-plane of this side. Hence the magnitude of the measured longitudinal wave signals can be maximized and the mode conversion from incident longitudinal wave to flexural wave at the step damage can be excluded in the measurements. This ensures the spectral element method developed based on the Love theory in Section 4 is able to well predict experimental measurements. The measured location was 450 mm from the piezoelectric transducer. The signal-to-noise ratio was improved by averaging the signals over a number of acquisitions. Finally the measured signals were fed into a computer via an oscilloscope (Tektronix TDS420A).

[Fig. 2. Schematic diagram of the experimental setup]

The step damage in each of the three beams was described by the damage location L_1, length L_2 and depth d as shown in Fig. 2. The step damages were manufactured using a milling machine, having been marked out manually. Hence, the measured uncertainty was ±1.0 mm for the damage location and length, and ±0.5 mm for the damage depth. All the cases are summarized in Table 1.

Case A considered damage located at $L_1 = 807.50$ mm with damage length and depth equal to 25.00 mm and 2.50 mm, respectively. Case B considered damage with greater damage length (L_2 = 65.50 mm) but smaller damage depth (d = 1.50 mm). The damage was

located at L_1 = 1097.25 mm. The last case, Case C, had the greatest damage length but the smallest damage depth. The damage was located at L_1 = 915.00 mm with L_2 = 90.00 mm and d = 1.10 mm.

[Table 1. Summary of all the damage cases in the experimental case studies]

The collected data from the experiments were used as the measured data in Eq. (3) of the proposed statistical framework. To achieve damage identification following the statistical framework, it requires a numerical model to predict the behavior of the guided wave signals in the damaged beams. Section 4 describes a computationally efficient spectral finite element model in detail.

4. Frequency domain spectral finite element method

4.1. Formulation of the spectral finite element

A computationally efficient spectral finite element method was used to model the longitudinal guided wave propagation in the damaged aluminum beams. The predicted longitudinal guided wave signals were then used in Eq. (3) of the proposed statistical framework for damage identification. The frequency domain spectral finite element method is essentially a finite element method formulated in the frequency domain. It significantly improves the computational efficiency of wave propagation simulation while retaining the same modeling flexibility as conventional finite element methods, and was used in the current study for identifying the damage using the proposed statistical framework.

In longitudinal wave propagation, beams not only deform longitudinally but also contract in transverse direction due to Poisson effect. The relationship between the transverse strain ε_y and the axial strain ε_x is described by $\varepsilon_y = -\nu\varepsilon_x$ where ν is the Poisson's ratio of the material. Love theory improves the elementary theory by accounting for this effect but still retains its simplicity. It is assumed that the kinetic energy is affected by the

transverse displacement due to the Poisson effect, but the strain energy still remains the same as the elementary theory.

[Fig. 3. Spectral element based on Love theory]

In the Love theory, a j-th beam element with length L_j as shown in Fig. 3 has two nodes with one longitudinal degree of freedom per node. The governing differential equation is [39]

$$E_j A_j \frac{\partial^2 u_j}{\partial x^2} + \nu_j^2 \rho_j J_j \frac{\partial^2}{\partial x^2}\left(\frac{\partial^2 u_j}{\partial t^2}\right) - \rho_j A_j \frac{\partial^2 u_j}{\partial x^2} = 0 \tag{8}$$

where $u_j = (x,t)$ is the longitudinal displacement within the j-th beam element. E_j and ρ_j are the Young's modulus and density of the material, respectively. J_j is the polar moment of inertia of the beam cross-section and A_j is the cross-sectional area. Based on the frequency spectral finite element method, the spectral representation of the longitudinal displacement is

$$u_j(x,t) = \sum_{n=1}^{N} \hat{u}_{n,j}(x,\omega_n) e^{i\omega_n t} \tag{9}$$

where $\hat{u}_{n,j}$ is the Fourier coefficients associated with the longitudinal displacement variable u_j at n-th angular frequency ω_n. i is the imaginary unit. The summation is carried out up to the Nyquist frequency ω_N. By substituting Eq. (9) into Eq. (8), the partial differential equations are reduced to an ordinary differential equation with the time variation removed as

$$E_j A_j \frac{d^2 \hat{u}_{n,j}}{dx^2} - \nu_j^2 \rho_j J_j \omega_n^2 \frac{\partial^2 \hat{u}_{n,j}}{\partial x^2} + \rho_j A_j \omega_n^2 \hat{u}_{n,j} = 0 \qquad \text{for } n = 1,...,N \tag{10}$$

The general longitudinal displacement variable in frequency domain is

$$\hat{u}_{n,j}(x,\omega_n) = U_{n,j} e^{-i(k_j x - \omega_n t)} \tag{11}$$

where $U_{n,j}$ is the amplitude of Fourier coefficients in spatial domain. Using Eqs. (10) and (11), the wavenumber $k_{n,j}$ is given by the relation

$$k_{n,j} = \pm\omega_n \sqrt{\frac{\rho_j A_j}{E_j A_j - \nu_j^2 \rho_j J_j \omega_n^2}} \tag{12}$$

The general longitudinal displacement at frequency ω_n is assumed in the form [39]

$$\hat{u}_{n,j} = C_{\alpha,j} e^{-k_{n,j}x} + C_{\beta,j} e^{-k_{n,j}\left(L_j - x\right)} \tag{13}$$

where $C_{\alpha,j}$ and $C_{\beta,j}$ are unknown coefficients to be determined from the boundary conditions at the left and right ends of the spectral element, where the longitudinal displacements as shown in Fig. 3 are

$$\hat{u}_{n,j}\left(0\right) = \hat{u}_{\alpha,j}, \quad \hat{u}_{n,j}\left(L_j\right) = \hat{u}_{\beta,j} \tag{14}$$

The relation between the longitudinal displacement and the unknown coefficients can be expressed in matrix form as

$$\begin{bmatrix} \hat{u}_{\alpha,j} \\ \hat{u}_{\beta,j} \end{bmatrix} = \begin{bmatrix} 1 & e^{-k_{n,j}L_j} \\ e^{-k_{n,j}L_j} & 1 \end{bmatrix} \begin{bmatrix} C_{\alpha,j} \\ C_{\beta,j} \end{bmatrix} = \mathbf{\Gamma}_{n,j} \begin{bmatrix} C_{\alpha,j} \\ C_{\beta,j} \end{bmatrix} \tag{15}$$

The nodal forces at left and right ends of the spectral element are

$$\hat{F}_{\alpha,j} = -\left(E_j A_j \frac{\partial \hat{u}_{\alpha,j}}{\partial x} - \nu_j^2 \rho_j J_j \omega_j^2 \frac{\partial \hat{u}_{\alpha,j}}{\partial x} \right) \tag{16}$$

$$\hat{F}_{\beta,j} = E_j A_j \frac{\partial \hat{u}_{\beta,j}}{\partial x} - \nu_j^2 \rho_j J_j \omega_j^2 \frac{\partial \hat{u}_{\beta,j}}{\partial x} \tag{17}$$

These nodal forces can be related to the unknown coefficients as

$$\begin{bmatrix} \hat{F}_{\alpha,j} \\ \hat{F}_{\beta,j} \end{bmatrix} = \begin{bmatrix} ik_{n,j}\left(E_j A_j - \nu_j^2 \rho_j J_j \omega_j^2\right) & -ik_{n,j}\left(E_j A_j - \nu_j^2 \rho_j J_j \omega_j^2\right) e^{-k_{n,j}L_j} \\ -ik_{n,j}\left(E_j A_j - \nu_j^2 \rho_j J_j \omega_j^2\right) e^{-k_{n,j}L_j} & ik_{n,j}\left(E_j A_j - \nu_j^2 \rho_j J_j \omega_j^2\right) \end{bmatrix} \begin{bmatrix} C_{\alpha,j} \\ C_{\beta,j} \end{bmatrix} = \mathbf{T}_{n,j} \begin{bmatrix} C_{\alpha,j} \\ C_{\beta,j} \end{bmatrix} \tag{18}$$

Using Eqs. (15) and (18), the relation between the nodal forces and the nodal displacements is given as

$$\begin{bmatrix} \hat{F}_{\alpha,j} \\ \hat{F}_{\beta,j} \end{bmatrix} = \mathbf{T}_{n,j} \mathbf{\Gamma}_{n,j}^{-1} \begin{bmatrix} \hat{u}_{\alpha,j} \\ \hat{u}_{\beta,j} \end{bmatrix} \tag{19}$$

The dynamics stiffness matrix $\mathbf{K}_{n,j}$ can be obtained by $\mathbf{T}_{n,j} \mathbf{\Gamma}_{n,j}^{-1}$.

In guided wave-based damage identification problems, the guided wave is generated from the excitation location and then propagates through the beams. If the beam length (e.g. 2 m long) is much longer than the wavelength of the excited guided wave (usually in the order

of millimeters), the wave reflected from the beam end can be neglected because of attenuation after a long travel distance or the reflected wave does not reach the desired location within the timeframe of the observation. In this situation the beam can be modeled as a semi-infinite or infinite beam.

Within the context of the frequency domain spectral finite element method, a throw-off element can be formulated to substantially reduce the computational cost of modeling the semi-infinite or infinite beam. This can be easily achieved by modifying Eq. (13). For example, if the wave is assumed to be propagating in a forward direction toward a non-reflecting boundary, the unknown constants $C_{\beta,j}$ that represent the reflected wave component travelling in a backward direction can be ignored to formulate the throw-off element. Following the same derivation procedure as Eqs. (15) to (19), the dynamic stiffness of the throw-off element is $\mathbf{K}^{0}_{n,j} = ik_{n,j}\left(E_j A_j - \nu_j^2 \rho_j J_j \omega_j^2\right)$.

4.2. Modeling of the damaged beam

The spectral finite elements formulated in Section 4.1 were used to model the damaged beams in the experiments discussed in Section 3. The damaged beam model was used to generate the predicted data in the statistical framework in Section 2. The quantitative damage identification was achieved by minimizing the discrepancy between the predicted and measured guided wave signals by changing the damage parameters of the damaged beam model. This section describes the modeling of the damaged beam.

The 2 m long damaged beams used in the experiment as described in Section 3 were modeled as spectral finite element models with three spectral finite elements and a throw-off element. The longitudinal guided wave was generated by applying the excitation in longitudinal direction using the same 80 kHz narrow-band excitation signal as discussed in Section 3. The length of the first spectral finite element was 450 mm; that is, the same as the measurement location, and hence, the longitudinal wave signals could be predicted by the nodal displacement of the element. The inspection region was 1 m from the measurement location.

The summation of the length of the first and second spectral finite elements represents the distance between the excitation location and the left end of the step damage, and it was defined as the damage location L_1. The third spectral finite element was used to simulate the step damage by reducing the beam depth, in which the length and depth reduction of the element were defined as the damage length L_2 and damage depth d. Finally the throw-off element was modeled as the end of the beam to simulate the semi-infinite condition.

It should be noted that although this study focuses on the step damage, the statistical framework is general and can be applied to identify different types of damages by employing different damage models in the spectral finite element method. As discussed in the Section 1, one of the objectives of the present study was to evaluate the accuracy and uncertainty of the signal processing techniques in the damage identification. Section 5 describes these signal processing techniques in detail.

5. Advanced signal processing techniques

Four signal processing techniques, Hilbert transform, Fourier transform and Gabor wavelet transform and discrete wavelet decomposition, were employed to process the guided wave data. These data were then used in the proposed statistical framework for damage identification. The damage identification results and the associated uncertainties were then compared and discussed in detail. The following sub-sections describe these signal processing techniques.

5.1. Hilbert transform

The Hilbert transform [3] of a guided wave signal in time domain $u(t)$ is defined as

$$h(t) = \frac{1}{\pi}\int_{-\infty}^{\infty} \frac{u(\tau)}{t-\tau} d\tau \tag{20}$$

where $h(t)$ is the Hilbert transform guided wave signal which is a signal with a 90° phase shift of $u(t)$. An analytic signal can be constructed by using the time signal $u(t)$ and the Hilbert transform signal $h(t)$ as

$$h_A(t) = u(t) + ih(t) = u_h(t)e^{i\phi(t)} \tag{21}$$

where i is the imaginary unit. $u_h(t)$ and $\phi(t)$ are the envelope and the instantaneous phase, respectively, and are defined as

$$u_h(t) = \sqrt{u^2(t) + h^2(t)}, \quad \phi(t) = \arctan\left[\frac{h(t)}{u(t)}\right] \tag{22}$$

In this study the signal envelope was used as the data in the proposed statistical framework in Eq. (3) for damage identification.

5.2. Fourier transform

Fourier transform enables the analysis of a signal in the frequency domain. The spectral amplitude was employed for damage identification [29,30]. The continuous Fourier transform of a guided wave signal $u(t)$ is defined as

$$\hat{u}(\omega) = \int_{-\infty}^{\infty} u(t)e^{-i\omega t}dt \tag{23}$$

where ω is the angular frequency. As the guided wave in time domain $u(t)$ is measured at N_t discrete sampling points as u_l for $(l = 1, 2, ..., N_t)$, the discrete Fourier transform was used as an alternative way of mathematically representing the continuous Fourier transform and is defined as

$$\hat{u}(\omega_n) = \sum_{n=1}^{N} u_l e^{-\frac{2\pi i}{N}nl} \tag{24}$$

In this study the Fourier transform was carried out using the Fast Fourier transform and the spectral amplitude $|\hat{u}(\omega_n)|$ was used as the data in Eq. (3) to identify the damages.

5.3. Gabor wavelet transform

Different to Fourier analysis, continuous wavelet transform provides a tool for time-frequency analysis of a signal. In wavelet transform the signal is broken down into local functions or wavelets. This is completely different from classical signal processing techniques, in which the signal is decomposed into global functions or harmonics. The

continuous wavelet transform [40,41] is defined as

$$CWT(a,b)=\frac{1}{\sqrt{a}}\int_{-\infty}^{\infty}u(t)\psi^{*}\left(\frac{t-b}{a}\right)dt \tag{25}$$

where a and b are the scaling parameter and translation parameter, respectively. $\psi(t)$ is the mother wavelet function. The asterisk denotes the complex conjugate. In this study the Gabor function [40,41] is chosen as the mother wavelet because it provides the balance between time and frequency resolution in the continuous wavelet transform. The Gabor function is defined as

$$\psi(t)=\frac{1}{\sqrt[4]{\pi}}\sqrt{\frac{\omega_0}{\lambda}}\exp\left[-\frac{(\omega_0/\lambda)^2}{2}t^2+i\omega_0 t\right] \tag{26}$$

where λ and ω_0 are the Gabor shaping factor and wavelet centre frequency, respectively. They influence the resolution in the time-frequency analysis and are usually chosen as $\lambda=\pi\sqrt{2/\ln 2}$ and 2π [40,41]. The Gabor wavelet transform of the signals represents the guided wave signals in the time-frequency domain with $t=b$ and $\omega=\omega_0/a$. In this study the absolute value of the continuous wavelet transform coefficient using the Gabor function at the excitation frequency is used as the data in Eq. (3) of the proposed statistical framework to identify the damages.

5.4. Discrete wavelet signal decomposition

In discrete wavelet transform, an orthonormal basis of function $\psi(t)$ can be obtained with dyadic translation and binary dilation by discretizing a and b in Eq. (25). The orthonormal basis of function $\psi(t)$ is defined as [40]

$$\psi_{m,d}(t)=2^{m/2}\psi\left(2^m t-d_w\right) \tag{27}$$

where the integers m and d_w are scale and translation indices. Using Eq. (27), the discrete wavelet transform can be written as

$$DWT(m,d)=\int_{-\infty}^{\infty}u(t)\psi_{m,d_w}(t)dt \tag{28}$$

The transform integral in Eq. (28) remains continuous but is determined only on a discretized

grid of a and b locations. The original signal can be reconstructed by summing the DWT coefficients to infinity over m and d_w. In the DWT ψ_{m,d_w} is an orthonormal dyadic discrete wavelet and is associated with scaling functions, which have the same form as the wavelet, given by

$$\varphi_{m,d}(t) = 2^{m/2}\varphi\left(2^m t - d_w\right) \tag{29}$$

and having property $\int_{-\infty}^{\infty}\varphi_{1,1}(t)dt = 1$. The scaling function can be convolved with the signal $u(t)$ to produce approximation coefficients $S_{m,d_w} = \int_{-\infty}^{\infty} u(t)\varphi_{m,d_w}(t)\,dt$. A signal $u(t)$ can be represented using the approximation coefficients and the detail coefficients as

$$u(t) = \sum_{d_w=-\infty}^{\infty} S_{m0,d_w}\varphi_{m0,d_w}(t) + \sum_{m=-\infty}^{m_0}\sum_{d_w=-\infty}^{\infty} DWT(m,d_w)\psi_{m,d_w}(t) \tag{30}$$

where m_0 is an arbitrary scale index. The detail coefficient at scale m is defined as $Q_m(t) = \sum_{d=-\infty}^{\infty} DWT(m,d_w)\psi_{m,d_w}(t)$. The approximation and detail coefficients at scale index $m+1$ can be calculated based on the coefficients at the previous scale as

$$S_{m+1,d_w} = \frac{1}{\sqrt{2}}\sum_q L_q S_{m,2d_w+q} \quad \text{and} \quad Q_{m+1,d_w} = \frac{1}{\sqrt{2}}\sum_q H_q S_{m,2d_w+q} \tag{31}$$

where $1/\sqrt{2}\,L_q$ and $1/\sqrt{2}\,H_q$ are low-pass and high-pass filter. The decomposition of the signal $u(t)$ into approximate and detail coefficients allows multi-resolution signal analysis. In guided wave problems the decomposed coefficients are commonly used for signal de-noising [42] or extracting information for damage identification [28].

In this study $\psi(t)$ was selected to be the 8th order Daubechies wavelet as it has been shown that its orthogonality and high regularity enables the detection of location properties in the signal [42] and has a close similarity to the excitation signal. The signal was decomposed into eight levels. The results showed that the sixth level approximation coefficients produce optimal complexity of the data while retaining optimum information of arrival time, length and magnitudes of the pulses. Hence the sixth level approximation coefficients were used as the data in Eq. (3) of the statistical framework for damage identification.

6. Results and discussions

6.1. Measured guided wave data and signal processing

All signals measured by the experimental setup described in Section 3 were normalized to have the unit amplitude of the incident wave. In this section the measured guided wave signal of Case A is used as an example to demonstrate the guided wave propagation and interaction at the damage, and discuss the signals processed using the signal processing techniques. Fig. 4 shows the measured guided wave of Case A. There were three wave packets after the incident wave. The incident wave was generated by the piezoceramic transducer located at the beam end. The incident wave passed through the measurement location and then reached the step damage. The first wave pulse shown in Fig. 4 is the incident wave. Two wave pulses were reflected when the incident wave was entering and leaving the step damage. These reflected pulses then propagated back to the beam end with the piezoceramic transducer installed and passed through the measurement location on the way. Wave packet 1 in Fig. 4 was formed by these wave pulses.

The pulses then rebounded at the beam end and propagated toward the measurement location again. Wave packet 2 shown in Fig. 4 was formed by these wave pulses. This wave packet then propagated toward the step damage. Similarly, wave reflection occurred at the step damage and the reflected pulses then passed through measurement location again and propagated toward the beam end where the piezoceramic transducer was installed. This is wave packet 3 as shown in Fig. 4.

[Fig. 4. Measured guided wave signal of Case A]

The measured guided wave signal was then processed using the signal processing techniques described in Section 5. It should be noted that the proposed damage identification method is a highly nonlinear optimization problem. The search space of Eq. (3) has a larger number of local optimums if the time domain guided wave signal is used directly in the damage identification. The signal processing techniques enhance the damage identification not only by extracting the damage information in the signal but also reducing the complexity

of the search space, i.e. reducing the number of local optimums.

Fig. 5 shows the signal envelope extracted by applying the Hilbert transform described in Section 5.1. The envelope of the wave signal is a curve that is tangent to every wave component of the wave signal. The envelope can be used to simplify the wave signal but it still retains the information of the arrival time, amplitude and width of the pulses. Fig. 6 shows the measured guided wave signal processed by the Fast Fourier transform described in Section 5.2. The signal was transformed from time domain to frequency domain. As the excitation is a narrow band pulse with a 80 kHz excitation frequency, the frequency of the measured guided wave signal shown in Fig. 4 spreads in a finite bandwidth with most components around the excitation frequency. Although the damage information is not explicitly shown in frequency domain, it still exists in the transformed data.

[Fig. 5. Hilbert transform guided wave signal of Case A]

[Fig. 6. Fast Fourier transformed guided wave signal of Case A]

Different to the Fast Fourier transform, the Gabor wavelet transform represents the measured guided wave in both the time and frequency domain. This provides a useful tool for analyzing non-stationary signals. Fig. 7 shows the Gabor wavelet transform spectrum of the measured guided wave signal as shown in Fig. 4. The horizontal and vertical axes are the time and frequency axis, respectively. The magnitude of the wavelet coefficients is represented on a color map. The color map indicates the wavelet coefficient distribution of the signal in time-frequency domain. As the excitation frequency is 80 kHz, the amplitude of the wavelet coefficients at this frequency are higher than those at other frequencies. Therefore, they were used in the damage identification.

[Fig. 7. Gabor wavelet transform spectrum of the guided wave signal in Case A (dashed line indicates the excitation frequency]

The discrete wavelet transform described in Section 5.4 is quite different from the continuous wavelet transform. The discrete wavelet transform decomposes the signal into different levels. Each level represents different frequency bandwidths. The results show that the sixth level approximate coefficient gives the optimal complexity of the data and hence it is employed in the damage identification. Fig. 8 shows the discrete wave decomposed approximate coefficient at the sixth level. As the data was compressed through discrete wavelet decomposition, the approximate coefficient was plotted using a line with markers to indicate the number of the data points. The discrete wavelet decomposed signal was then employed in the damage identification using the proposed statistical approach.

[Fig. 8. Discrete wavelet decomposed guided wave signal of Case A]

6.2. Damage identification results

The measured guided wave signals in Cases A to C as shown in Table 1 were processed using the signal processing techniques described in Section 5. The processed signals were then employed in the proposed statistical framework to identify the damages. Table 2 summarizes the results of the damage identification using the time domain signal and the signal processed using the Hilbert transform, Fourier transform, Gabor wavelet transform and discrete wavelet decomposition in Case A. The corresponding percentages of errors were calculated and are shown in the square brackets. The damage identification results of using the time domain signal show that although the identified damage location L_1 = 826.16 mm has reasonable agreement with the true damage location, the results incorrectly identify the damage length and depth.

As shown in Fig. 4, there was a small additional wave pulse right after the incident wave in Case A because the piezoceramic transducer was not attached perfectly parallel to the surface of the beam end. In these circumstances, it was found that the use of the time domain signal made it difficult to accurately identify the damage parameters, especially the damage

length and depth. The total error was calculated by taking the average of the percentage of error in the identified damage location, length and depth. These calculations provided a way, in which the damage identification results achieved by using different signal processing techniques, could be compared. The averaged error for the results of using the time domain signal was 57.70% as shown in Table 2.

Table 2 also lists the damage identification results of the signal processed using Fast Fourier transform. But the accuracy was less than when using the time domain signal directly. The average percentage of error was 102.82%. The last three columns of Table 2 show the results of the signals processed using the Hilbert transform, Gabor wavelet transform and discrete wavelet decomposition. These results are similar in terms of accurately identifying the damage, and the corresponding averaged percentages of errors are 9.77%, 10.12% and 9.59%, respectively. The averaged percentage of error is much smaller than the results of using the time domain signal.

The results of Case A show that the signal processing techniques, such as Hilbert transform, Gabor wavelet transform and discrete wavelet decomposition, are able to enhance the damage identification for guided wave signals collected under imperfect conditions.

[Table 2. Damage identification results of Case A]

[Table 3. Damage identification results of Case B]

The results of Cases B and C are summarized in Tables 3 and 4, respectively. These two cases involved damages at different locations with different damage lengths and depths. The cases provided the opportunity to conduct a comprehensive study of the performance of the signal processing techniques in damage identification. Case B involved a step damage having a longer length but less depth than Case A. The damage identification results are shown in Table 3.

Similar to Case A, the damage identification results from using the Fast Fourier

transform produced the least accurate identification of the damage. The results of the Hilbert transform and discrete wavelet decomposition are not of the same quality as the time domain signal in terms of damage identification. However, the results from the Gabor wavelet transform produced the most accurate identification of the damage. The identified damage parameters were L_1 = 1057.98 mm L_2 = 65.28 mm and d = 1.59 mm and the corresponding percentages of errors were 3.58%, 0.33% and 5.93%. The averaged percentage of error was only 3.28%.

[Table 4. Damage identification results of Case C]

Case C considers a step damage with the greatest damage length (L_2 = 90.00 mm) but the smallest damage depth (d = 1.10 mm) among the three damage cases. The same as Cases A and B, the results of the signals processed using the Fast Fourier transform displayed the largest average percentage of error in the damage identification. It is fair to conclude, therefore, that using the Fast Fourier transform to process guided wave signals produces the least accurate damage identification in the study.

In Case C the results from the time domain signal are in good agreement with the true damage location, length and depth. However, the accuracy cannot match that achieved by using the Hilbert transform, Gabor wavelet transform and discrete wavelet decomposition, especially in identifying the damage length and depth. As in Case B, the Gabor wavelet transform performed best in terms of damage identification. The averaged percentage of error was only 1.63% in Case C.

Overall the results of Cases A to C show that processing guided wave signals with the Fast Fourier transform produces insufficiently accurate results when it comes to damage identification. The time domain signal can be used to more accurately identify damages, but only if the piezoceramic transducers are installed almost perfectly. The signal processing techniques, Hilbert transform, Gabor wavelet transform and discrete wavelet decomposition, were all able to enhance the accuracy of damage identification, but overall, it was found that

the Gabor wavelet transform performed best.

6.3. Uncertainty analysis

The uncertainties associated with the damage identification results were also quantified using the proposed statistical framework. This analysis provided a further comparison of the performance of the signal processing techniques in damage identification. As discussed in Section 2, the uncertainties associated with the damage identification results were quantified by calculating the posterior PDF of the damage parameters.

As an example, Fig. 9 shows the normalized marginal PDF of the damage length and depth for the signal processed using the Hilbert transform, Gabor wavelet transform and discrete wavelet decomposition in Case C. The figure shows that the rate of the PDF value drops when one moves away from the identified value of the damage length and depth. The figure indicates the level of confidence that can be placed in the identification of the damage length and depth. For easier comparison of the results, the marginal cumulative distribution of one of the damage parameters can be calculated by integrating the posterior PDF with respect to the other damage parameters.

As an example, Fig. 10 shows the marginal cumulative distribution of the damage depth for the signal processed using the Hilbert transform, Gabor wavelet transform and discrete wavelet decomposition. The slope of the curve is a measure of the uncertainty associated with the identified value. As shown in Fig. 10, the identified damage depth of using the signal processed by the discrete wavelet decomposition has the flatter curve, which means it exhibits greater uncertainty.

[Fig. 9. Normalized marginal PDF of the damage length and depth for the signal processed using a) Hilbert transform, b) Gabor wavelet transform and c) discrete wavelet decomposition in Case C]

[Fig. 10. Marginal cumulative distribution of the damage depth for the signal processed

using Hilbert transform (solid line), Gabor wavelet transform (dashed line) and discrete wavelet decomposition (dotted line)]

To provide a more quantitative comparison of the uncertainties associated with the damage identification results, the coefficient of variation (COV) of the identified damage location, length and depth were calculated for Cases A, B and C and also listed in the brackets of Tables 2, 3 and 4, respectively. Overall the uncertainties of the results using the signals processed by the Gabor wavelet transform have smaller COV values in most of the situations, especially for the identified damage length and depth. Based on the accuracy of the damage identification results and the associated uncertainties, it can be concluded that the Gabor wavelet transform offers superior performance, enhancing the ability of the proposed statistical approach to damage identification.

7. Conclusions

The current study reported in this paper applied advanced signal processing techniques for damage identification in beams using longitudinal guided waves. The proposed statistical approach provides quantitative identification of the damages based on the longitudinal guided wave signal measured at a single location. One of the attractive advantages of the proposed statistical approach is that it also quantifies the uncertainties associated with the damage identification results, which provides essential information for engineers in making judgments on the remedial work.

Four signal processing techniques, including the Fast Fourier transform, Hilbert transform, Gabor wavelet transform and discrete wavelet decomposition, were used to process the guided wave signals for damage identification. The accuracy and uncertainty of the damage identification results using each of the signal processing techniques were compared and discussed in detail.

The experimental investigation verified that frequency domain guided wave signals processed by the Fast Fourier transform are not suitable for damage identification in the

context of the proposed statistical approach. On the other hand, the results demonstrated that the Hilbert transform, Gabor wavelet transform and discrete wavelet decomposition are able to enhance the results produced by the guided wave signals. Overall, however, the damage identification results provided by the signals and processed by the Gabor wavelet transform, in combination with the statistical analysis of the results, proved superior to other signal processing techniques in terms of accurately identifying the location, length and size of the damage, as well as the level of uncertainty inherent in the damage identification.

8. Acknowledgements

This work was supported by the Australian Research Council under grant number DE130100261. The support is greatly appreciated. The author would like to acknowledge A/Prof. Martin Veidt for his support of accessing the equipments at the University of Queensland during the visit.

9. References

[1] Sohn H, Farrar CR, Hemez FM, Shunk DD, Stinemates DW, Nadler BR. A review of structural health monitoring literature from 1996-2001. Los Alamos National Laboratory. Los Alamos, N.M 2004; Report no. LA-13976-MS.

[2] Friswell MI. Damage identification using inverse methods. Phil Trans R Soc A 2007; 365: 393-410.

[3] Staszewski WJ, Boller C, Tomlinson G. Health monitoring of aerospace structures: smart sensor technologies and signal processing, West Sussex, Wiley 2004.

[4] Worden K, Farrar CR, Manson G, Park G. The fundamental axioms of structural health monitoring. Phil Trans R Soc A 2007; 463: 1639-1664.

[5] Kim JT, Ryu YS, Cho HM, Stubbs N. Damage identification in beam-type structures: frequency-based method vs mode-shape-based method. Eng Struct 2003; 25: 57-67.

[6] Ko JM, Ni YQ. Technology developments in structural health monitoring of large-scale

bridges. Eng Struct 2005; 27: 1715-1725.

[7] Lam HF, Ng CT, Veidt M. Experimental characterization of multiple cracks in a cantilever beam utilizing transient vibration data following a probabilistic approach. J Sound Vib 2007; 305: 34-49.

[8] Lam HF, Ng CT. A probabilistic method for the detection of obstructed cracks of beam-type structures using spatial wavelet transform. Prob Eng Mech 2008; 23: 237-245.

[9] Lam HF, Ng CT. The selection of pattern features for structural damage detection using an extended Bayesian ANN algorithm. Eng Struct 2008; 30: 2762-2770.

[10] Weng JH, Loh CH, Lynch JP, Lu KC, Lin PY, Wang Y. Output-only modal identification of a cable-stayed bridge using wireless monitoring systems. Eng Struct 2008; 30: 1820-1830.

[11] Lam HF, Ng CT, Leung AYT. Multicrack detection on semirigidly connected beams utilizing dynamic data. J Eng Mech ASCE 2008; 134: 90-99.

[12] Raghavan, A, Cesnik CES. Review of guided-wave structural health monitoring. Shock Vib Digest 2007; 39: 91-114.

[13] Nair A, Cai CS. Acoustic emission monitoring of bridges: review and case studies. Eng Struct 2010; 32: 1704-1714.

[14] Park G, Sohn H, Farrar CR, Inman DJ. Overview of piezoelectric impedance-based health montoirng and path forward. Shock Vib Digest 2003; 35: 451-463.

[15] Grahn T, Lamb wave scattering form a circular partly through-thickness hole in a plate. Wave Motion 2003; 37: 63-80.

[16] Wang CH, Chang FK. Scattering of plate waves by a cylindrical inhomogeneity. J Sound Vib 2005; 282: 429-451.

[17] Veidt M, Ng CT. Scattering characteristics of Lamb waves form debondings at structural features in composite laminates. J Acoust Soc Am 2012; 132: 115-123.

[18] Ng CT, Veidt M. Scattering of the fundamental anti-symmetric Lamb wave at delaminations in composite laminates. J Acout Soc Am 2011; 129: 1288-1296.

[19] Moreau L, Caleap M, Velichko A, Wilcox PD. Scattering of guided waves by

through-thickness cavities with irregular shapes. Wave Motion 2011; 48: 586-602.

[20]Ng CT, Veidt M, Rose LRF, Wang CH. Analytical and finite element prediction of Lamb wave scattering at delaminations in quasi-isotropic composite laminates. J Sound Vib 2012; 331: 4870-4883

[21]Giurgiutiu V, Bao JJ. Embedded-ultrasonic structural radar for in situ structural health monitoring of thin-wall structures. Struct Health Monitor 2004; 121: 121-140.

[22]Zhao X, Gao H, Zhang G, Ayhan B, Yan F, Kwan C, Rose JL. Active health monitoring of an aircraft wing with embedded piezoelectric sensor/actuator network: I defect detection, localization and growth monitoring. Smart Mater Struct 2007; 16: 1208-1217.

[23]Ng CT, Veidt M. A lamb-wave-based technique for damage detection in composite laminates. Smart Mater Struct 2009; 18(074006): 1-12.

[24]Wang L, Yuan FG. Damage identification in a composite plate using prestack reverse-time migration technique. Struct Health Monitor 2005; 4: 195-211.

[25]Ng CT, Veidt M, Rajic N. Integrated piezoceramic transducers for imaging damage in composite laminates. Proc of SPEI 2009; 7493: 74932M-1-8.

[26]Rose LRF, Wang CH. Mindlin plate theory for damage detection: imaging of flexural inhomogeneities. J Acoust Soc Am 2010; 127: 754-763

[27]Garg AK, Roy Mahapatra D, Suresh S, Gopalakrishnan S, Omkar SN. Estimation of composite damage model parameters using spectral finite element and neural network. Comp Sci Tech 2004; 64: 2477-2493.

[28]Liew CK, Veidt M. Pattern recognition of guided waves for damage evaluation in bars. Pattern Recog Letters 2009; 30: 321-330.

[29]Nag A, Roy Mahapatra D, Gopalakrishnan S. Identification of delamination in composite beams using spectral estimation and a genetic algorithm. Smart Mater Struct 2002; 11: 899-908.

[30]Krawczuk M. Application of spectral beam finite element with a crack and iterative search technique for damage detection. Finite Elem Analy Design 2002; 38: 537-548.

[31]Ng CT, Veidt M, Lam HF. Guided wave damage characterization in beams utilizing

probabilistic optimization. Eng Struct 2009; 31: 2842-2850.

[32]Pau A, Vestroni F. Wave propagation in one-dimensional waveguides for damage characterization. J Intell Mater Syst Struct 2011; 22: 1869-1877.

[33]Staszewski WJ. Advanced data pre-processing for damage identification based on pattern recognition. Inter J Syst Sci 2002; 31: 1381-1396.

[34]Yu L, Giurgiutiu V. Advanced signal processing for enhanced damage detection with piezoelectric wafer active sensors. Smart Struct Syst 2005; 1: 185-215.

[35]Beck, JL and Katafygiotis, LS. Updating models and their uncertainties I: Bayesian statistical framework. J Eng Mech ASCE 1998; 124: 455-461.

[36]Papadimitriou C, Beck JL, Katafygiotis LS. Asymptotic expansions for reliability and moments of uncertain systems. J Eng Mech ASCE 1997; 123: 1219-1229.

[37]Kennedy J, Eberhart RC. Particle swarm optimization. In Proc IEEE Inter Conf Neural Networks IV, Piscataway, IEEE 1995; 1942-1948.

[38]Perez RE, Behdinan K. Particle swarm approach for structural design optimization. Comp Struct 2007; 85: 1579-1588.

[39]Doyle JF. Wave propagation in structures spectral analysis using fast discrete Fourier transforms, 2ed, Springer, 1997.

[40]Kishimoto K, Inoue H, Hamada M, Shibuya T. Time frequency analysis of dispersive waves by means of wavelet transform. J Appl Mech 1995; 62: 841-848.

[41]Veidt M, Ng CT. Influence of stacking sequence on scattering characteristics of the fundamental anti-symmetric Lamb wave at through holes in composite laminates. J Acoust Soc Am 2011; 129: 1280-1287.

[42]Staszewski WJ, Pierce SG, Worden K, Philp WR, Tomlinson GR, Culshaw B. Wavelet signal processing for enhanced Lamb-wave defect detection in composite plates using optical fiber detection. Opt Eng 1997; 36: 1877-1888.

Figures List

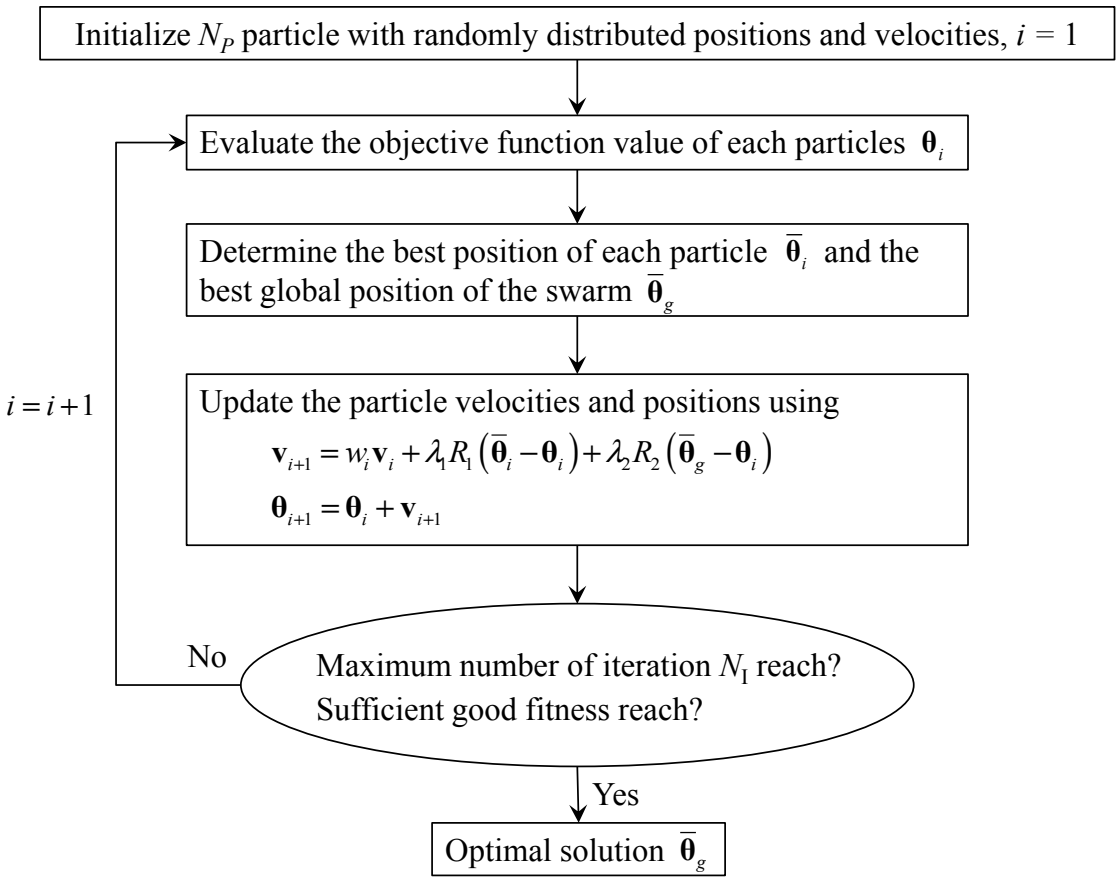

Fig. 1. Flowchart of PSO algorithm

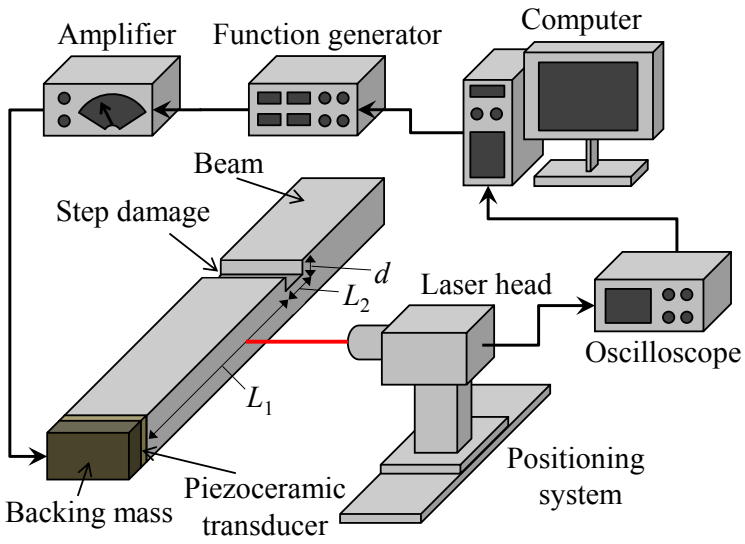

Fig. 2. Schematic diagram of the experimental setup

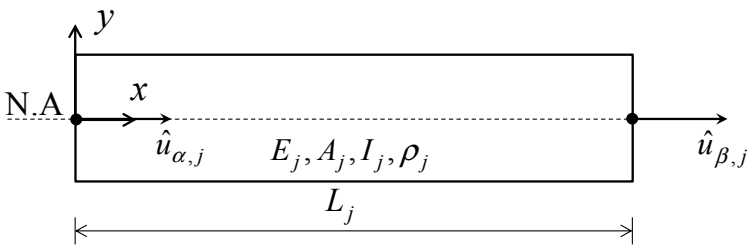

Fig. 3. Spectral element based on Love theory

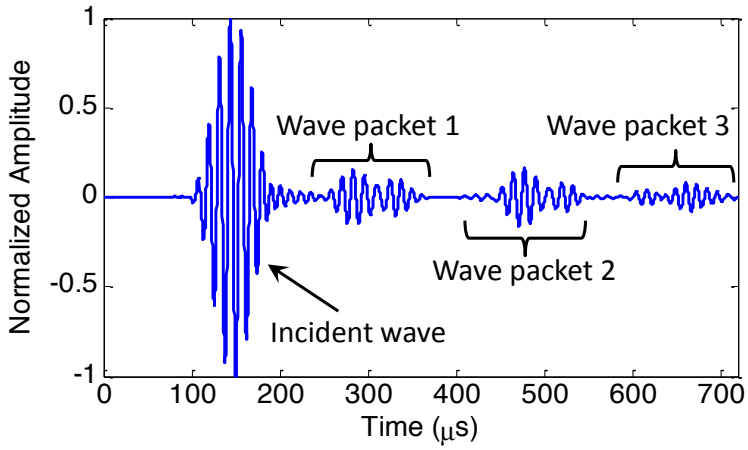

Fig. 4. Measured guided wave signal of Case A

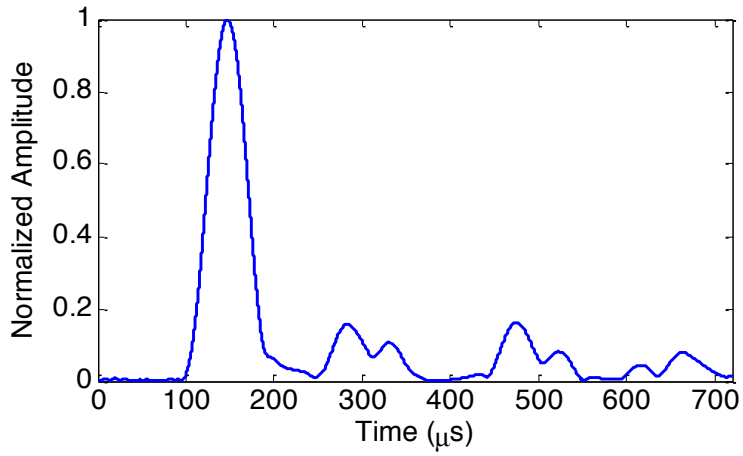

Fig. 5. Hilbert transformed guided wave signal of Case A

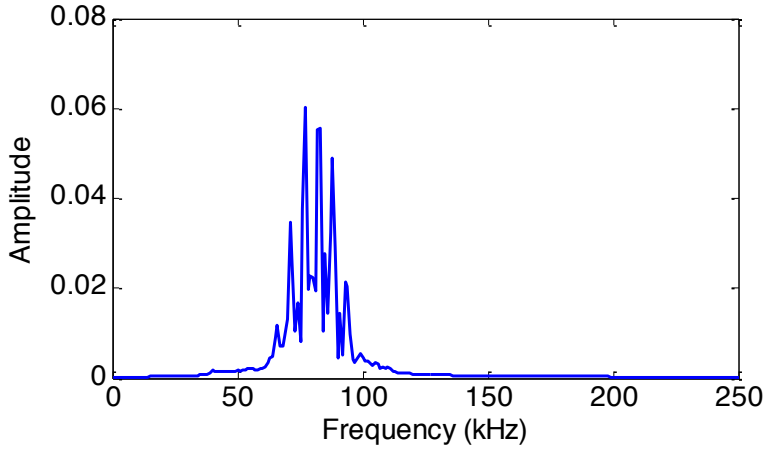

Fig. 6. Fast Fourier transformed guided wave signal of Case A

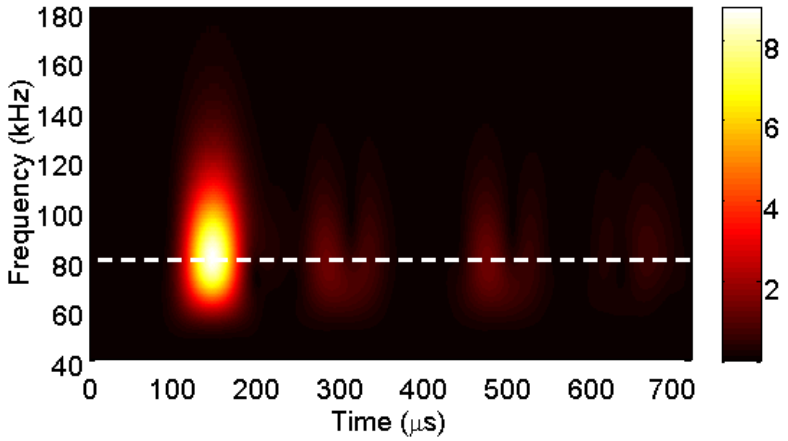

Fig. 7. Gabor wavelet transform spectrum of the guided wave signal in Case A (dashed line indicates the excitation frequency)

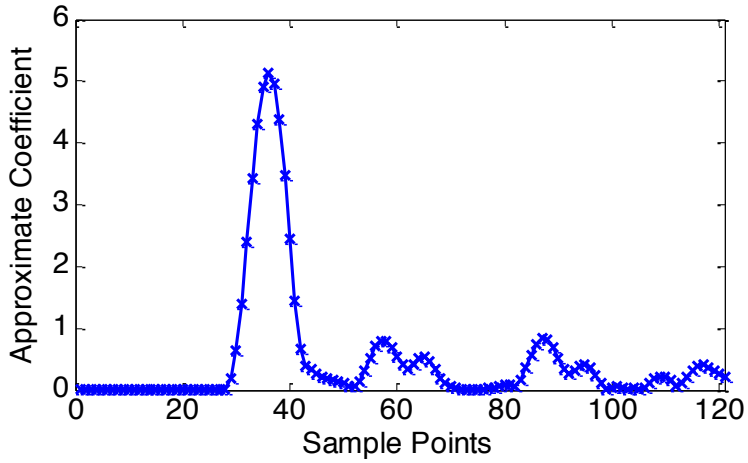

Fig. 8. Discrete wavelet decomposed guided wave signal of Case A

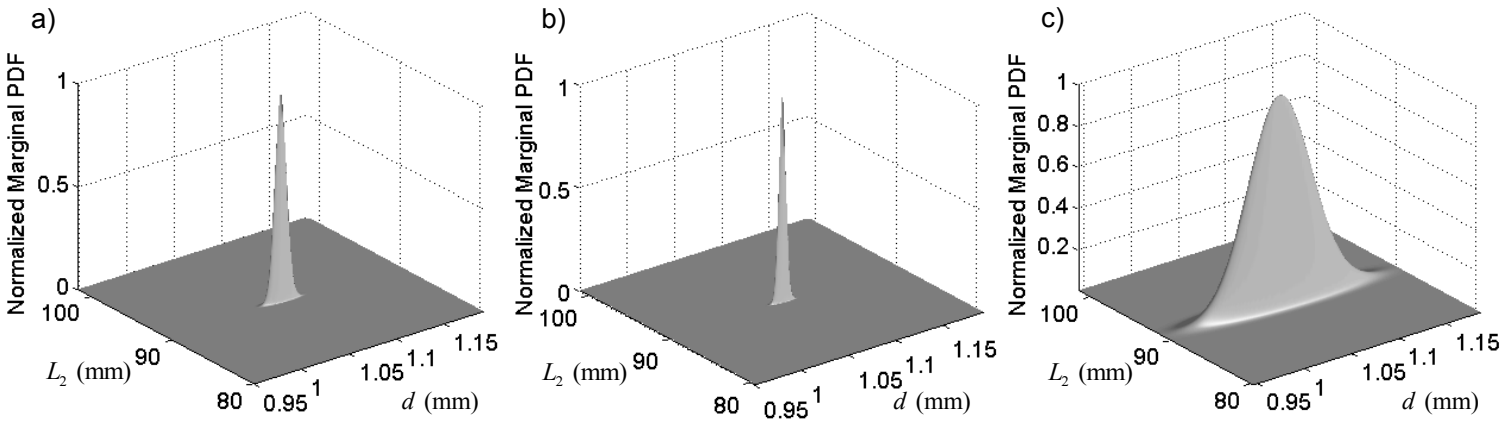

Fig. 9. Normalized marginal PDF of the damage length and depth for the signal processed using a) Hilbert transform, b) Gabor wavelet transform and c) discrete wavelet decomposition in Case C

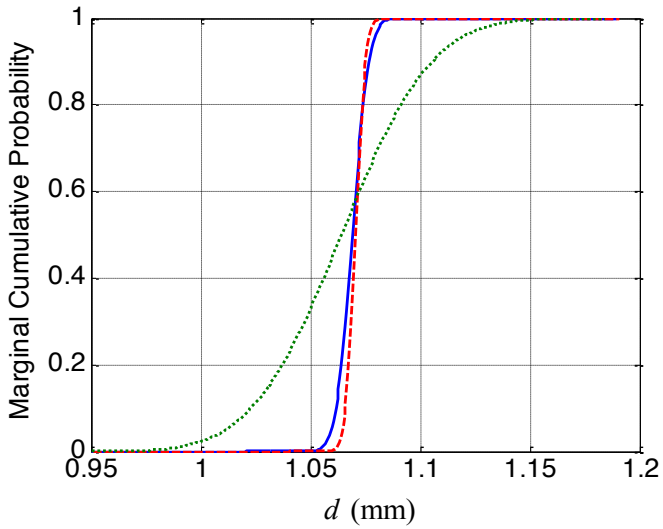

Fig. 10. Marginal cumulative distribution of the damage depth for the signal processed using Hilbert transform (solid line), Gabor wavelet transform (dashed line) and discrete wavelet decomposition (dotted line)

Tables List

Table 1. Summary of all the damage cases in the experimental case studies

	Case A	Case B	Case C
Damage location (L_1) (mm)	807.50±1	1097.25±1	915.00±1
Damage length (L_2) (mm)	25.00±1	65.50±1	90.00±1
Damage depth (d) (mm)	2.50±0.5	1.50±0.5	1.10±0.5

Table 2. Damage identification results of Case A

	Time domain signal	Fast Fourier transform	Hilbert transform	Gabor wavelet transform	Discrete wavelet decomposition
L_1 (mm)	826.16	794.36	798.74	799.81	799.19
[error]	[2.31%]	[1.63%]	[1.09%]	[0.95%]	[1.03%]
(COV)	(0.01%)	(0.19%)	(0.04%)	(0.05%)	(0.29%)
L_2 (mm)	59.53	87.78	28.55	28.58	28.55
[error]	[138.13%]	[251.12%]	[14.18%]	[14.33%]	[14.20%]
(COV)	(0.16%)	(1.22%)	(0.09%)	(0.08%)	(0.49%)
d (mm)	1.68	1.11	2.85	2.88	2.84
[error]	[32.68%]	[55.70%]	[14.04%]	[15.09%]	[13.53%]
(COV)	(1.46%)	(11.70%)	(0.42%)	(0.38%)	(2.63%)
Averaged error	57.70%	102.82%	9.77%	10.12%	9.59%

Table 3. Damage identification results of Case B

	Time domain signal	Fast Fourier transform	Hilbert transform	Gabor wavelet transform	Discrete wavelet decomposition
L_1 (mm)	1118.26	1057.01	1055.52	1057.98	1055.50
[error]	[1.92%]	[3.67%]	[3.80%]	[3.58%]	[3.81%]
(COV)	(0.01%)	(0.11%)	(0.05%)	(0.05%)	(0.33%)
L_2 (mm)	68.12	33.76	79.51	65.28	79.50
[error]	[4.01%]	[48.46%]	[21.39%]	[0.33%]	[21.38%]
(COV)	(0.18%)	(0.90%)	(0.17%)	(0.16%)	(1.12%)
d (mm)	1.67	3.00	1.39	1.59	1.38
[error]	[11.14%]	[100.00%]	[7.50%]	[5.93%]	[7.83%]
(COV)	(1.39%)	(6.21%)	(0.60%)	(0.77%)	(4.03%)
Averaged error	5.69%	50.71%	10.90%	3.28%	11.01%

Table 4. Damage identification results of Case C

	Time domain signal	Fast Fourier transform	Hilbert transform	Gabor wavelet transform	Discrete wavelet decomposition
L_1 (mm)	933.82	1076.75	895.42	896.17	894.37
[error]	[2.06%]	[17.68%]	[2.14%]	[2.06%]	[2.26%]
(COV)	(0.01%)	(0.11%)	(0.03%)	(0.03%)	(0.23%)
L_2 (mm)	93.28	66.33	90.64	90.17	90.49
[error]	[3.65%]	[26.30%]	[0.72%]	[0.19%]	[0.55%]
(COV)	(0.16%)	(0.77%)	(0.12%)	(0.07%)	(0.57%)
d (mm)	1.02	2.55	1.07	1.07	1.06
[error]	[6.97%]	[131.41%]	[2.78%]	[2.66%]	[3.23%]
(COV)	(1.99%)	(5.68%)	(0.55%)	(0.34%)	(3.02%)
Averaged error	4.23%	58.46%	1.88%	1.63%	2.01%